AAS 19-064

SEXTANT NAVIGATION ON THE INTERNATIONAL SPACE STATION: A HUMAN SPACE EXPLORATION DEMO

Greg N. Holt*, Brandon Wood†

Astronauts on board the International Space Station (ISS) tested a hand-held sextant to demonstrate potential use on future human exploration missions such as Orion and Gateway. The investigation, designed to aid in the development of emergency navigation methods for future crewed spacecraft, took place from June-December 2018. A sextant provides manual capability to perform star/planet-limb sightings and estimate vehicle state during loss of communication or other contingencies. Its simplicity and independence from primary systems make it useful as an emergency survival backup or confirming measurement source. The concept of using a sextant has heritage in Gemini, Apollo, and Skylab. This paper discusses the instrument selection, flight certification, crew training, product development, experiment execution, and data analysis. Preflight training consisted of a hands-on session with the instrument and practice in a Cupola mock-up with star field projector dome. The experiment itself consisted of several sessions with sextant sightings in the ISS Cupola module by two crew members. Sightings were taken on star pairs, star/moon limb, and moon diameter. The sessions were designed to demonstrate star identification and acquisition, sighting stability, accuracy, and lunar sights. Results are presented which demonstrate sightings within the accuracy goal of 60 arcseconds, even in the presence of window refraction effects and minimal crew training. The crew members provided valuable feedback on sighting products and microgravity stability techniques.

INTRODUCTION

A manual, crew-operated method for backup and emergency navigation on lunar flights has been proposed since the early planning of such missions. Theoretical approaches to manual space navigation were presented in the 1960s by authors such as Nordtvedt[1] and Havill,[2] and recently by Zanetti.[3] Early '60s tests at NASA Ames using simulators and aircraft are described in Lampkin and Randle,[4] and a Gemini XII flight experiment is documented in Smith.[5] The Apollo Space Sextant design and operation are described in Battin[6] and Brennan.[7] Comparable Soviet designs were also well under development prior to their lunar program cancellation, as described in Eneev.[8]

Ground-based radiometric and computer-automated optical methods are available in the current state of the art, and will likely be the primary means of navigating lunar missions in the foreseeable future. However, astronauts aboard spacecraft such as the Orion Crew Exploration Vehicle could benefit from a decidedly "low-tech" approach for contingencies where communications or flight computers are compromised. One of the primary differences in this study versus previous manual navigation efforts is its focus solely as an emergency backup, where the proposed method gives the crew an opportunity to effect their own rescue. The recent investigation of this method began in

*NASA Orion Navigation Lead, Johnson Space Center, 2101 NASA Parkway, Houston, TX, 77058
†Navigation Engineer, Johnson Space Center, 2101 NASA Parkway, Houston, TX, 77058

2015[9] as the initial part of a ground, low-earth orbit, and cislunar test progression. From this initial ground characterization, the test moved to in-space demonstration with the International Space Station (ISS) experiment as shown in Figure 1. If shown feasible, this would lead the way to its demonstration on a crewed lunar mission as a method of emergency return navigation.

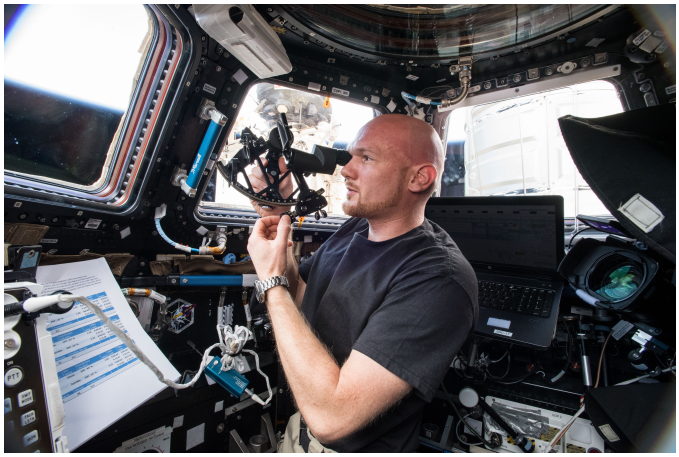

Figure 1. ESA Astronaut Alexander Gerst Performing a Sighting Session

INSTRUMENT AND FLIGHT CERTIFICATION

The flight instrument was a Celestaire Astra III Professional hybrid brass/aluminum sextant, serial number 1183118. It was outfitted with a 7x35, 6.5° field-of-view prism telescope for sighting. The manufacturers calibration certificate is dated Feb 11, 2015 and indicates performance within 0.1 arcmin in the regions as indicated in Table 1. This model was chosen based on results from the 2015 study[9] for its accuracy (achieved by the superior machining tolerances of the brass arc vs. aluminum) combined with the lower mass and slightly more compact construction of the aluminum frame than a solid brass instrument. A spare telescope, horizon mirror, and index mirror were flown for the experiment as well as a microfiber cleaning cloth, adjustment wrench, and screwdriver. A lanyard was included but was not used by the crew, as they indicated it was not needed in microgravity and having hook-and-loop fastener tape on the handle was more useful for temporarily securing the sextant to a wall if needed.

Table 1. Manufacturers Calibration Report for ISS Sextant Instrument

Angle	0°	10°	20°	30°	40°	50°	60°	70°	80°	90°	100°	110°	120°
Correction	0’	0’	0’	-0.1’	-0.1’	-0.1’	-0.1’	-0.1’	-0.1’	-0.1’	-0.1’	-0.1’	0’

The model of sextant instrument used is shown in Figure 2. Flight certification required evaluating and documenting all the components for acceptable characteristics of flammability, outgassing, fracture, etc. The main safety concern for use on ISS was breakage of the glass or mirror components during vibration loads, so it was placed in two plastic bags and stowed in protective foam for launch as shown in Figure 3. The crew reported the instrument had no damage upon first unpack and inspection on-orbit.

Figure 2. Astra IIIB Pro Sextant Used for the Experiment (trainer unit shown)

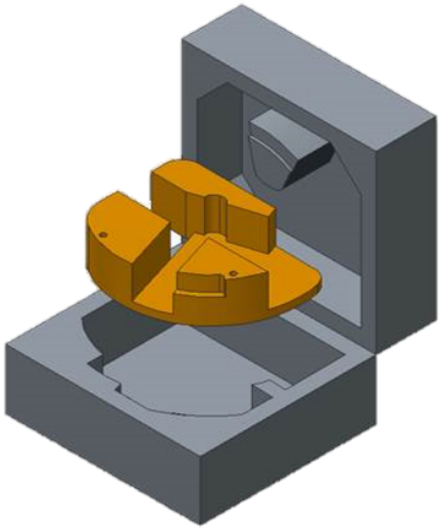

Figure 3. Stowage Foam for Launch

TRAINING

A space station crew has a very busy schedule in preparation for flight, so training time is limited. The experiment team was able to procure one hour of ground training time with the crew prior to flight, since it was clear that having an instructor walk them through the first use of the sextant would be beneficial. Although this is considered very limited training, it certainly provides a conservative representation of what a minimally trained crew member can accomplish. Ideally the training would have been conducted with a live night sky where actual stars and/or the moon could be observed, but again the limited timeframe and availability of the crew forced an indoor alternative. Training was therefore conducted in the Space Environment Simulator (SES()) at NASA Johnson Space Center, which contains a mockup of the ISS Cupola module and a dome projection system capable of generating a variety of Earth/starfield views for training. After a briefing on the experiment and parts of the sextant, the crew was given hands-on instruction in use of the instrument as shown in Figure 4. The first sights were taken with two laser-projected dots on the training facility wall to get the mechanics of zeroing, orienting, and acquiring. Training then moved to the SES Alpha Dome/Cupola mockup, shown in Figure 5. Several simulated star pairs were given to practice identification and sighting in the confines of the Cupola with the Earth and ISS structure taking up large portions of the window field of view. The sights were evaluated and immediate feedback given to the crew, who were able to quickly begin taking sights with errors within the expected parallax effect for a projection dome of that size.

Figure 4. Sextant Navigation Crew Training

Figure 5. Crew Training in the SES Alpha Dome

FLIGHT PRODUCTS

A full-sky star chart was provided for the crew as shown in Figures 6 and 7. The star chart was a modified version of the standard US Naval Observatory product for the Nautical Almanac. During the first session, the crew noted that this chart was not ideal for the narrow field of view they experienced with the obscuration from the Earth limb and ISS structure. For subsequent sessions, a tailored star chart for specific star pairs was provided as shown in Figure 8, which includes predicted star pair angular separations corrected for proper motion. An analysis simulation was built in FreeFlyer for real-time operation and product developement, and exported Cupola window views were used for the products. The analysis simulation was also used to screen viewing opportunities months at a time for favorable window/star/moon geometry. When a day was determined, sighting predicts were produced and verified by the ISS Pointer flight controllers. Then visualizations were produced and converted to night-vision-friendly star charts.

EXPERIMENT SESSIONS

The experiment was launched to ISS on the Orbital Sciences Cygnus cargo resupply mission OA-9 as seen in Figure 9. The crew used the instrument to conduct the experiment as seen in Figures 1 and 10. The payload developers were live on space-to-ground, and live video was downlinked during the sessions. Six sessions were conducted in total. A generic session typically consisted of 30 minutes preparation to unpack, inspect, and check the sextant calibration, set up the video and

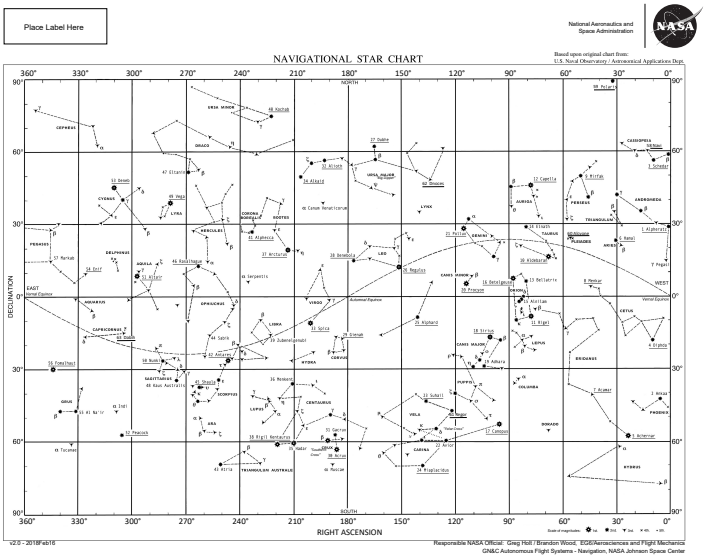

Figure 6. Star Chart Front

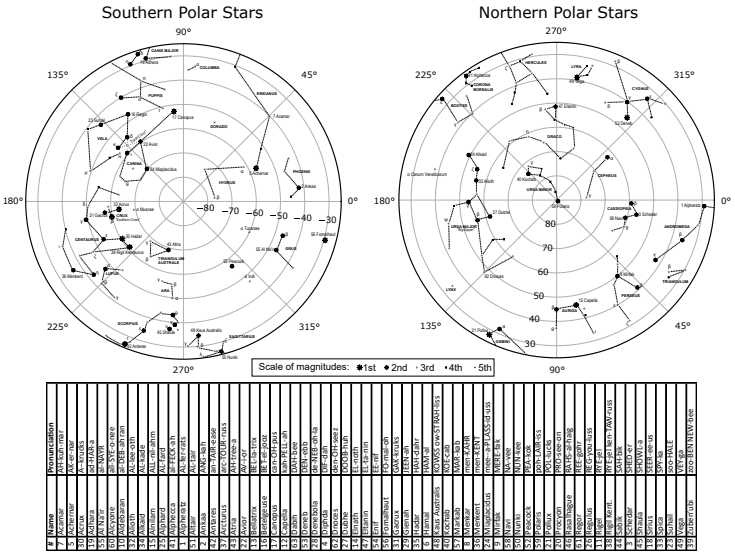

Figure 7. Star Chart Reverse

audio downlink, and review the star charts for the activity. Once orbital night arrived, the crew had approximately 30 minutes to take the measurements. After orbital sunrise, 10 minutes was reserved to debrief the crew and stow the equipment. The sessions were designated by their 2018 day-of-year starting epoch in Greenwich Mean Time, for example GMT179 for June 28.

In the first session conducted on GMT179, the crew re-familiarized themselves with the instrument on orbit. It was implemented as a joint "train-by-procedure" exercise, with the crew working together through a sighting session with coaching from the ground. The main skills to refresh were

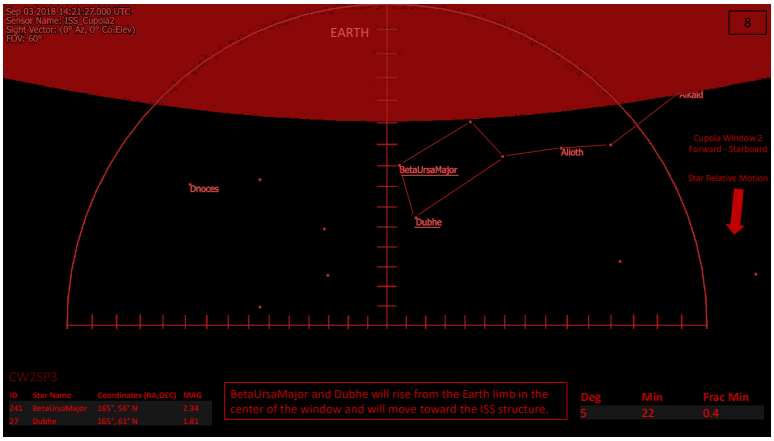

Figure 8. Sample Crew Message Star Chart for Real-Time Use

Figure 9. Launch of Orbtial OA-9 Resupply Mission with Sextant Navigation Payload

star identification and acquisition with the sextant. This session was conducted with the whole sky starchart, however the crew provided feedback that the narrow swath of open space between the Earth limb and the ISS structure made identification of stars from the whole sky chart difficult. The custom narrow-field star chart was used in all subsequent tests. The sextant was inspected and calibrated, and after some initial difficulty in star identification the crew was able to take good readings on a star pair and lunar diameter. The instrument retained a small bit of side error (estimated on the order of 2-3 arcsec) which the crew was unable to remove. The index error for individual crew members was measured before and after each session. The crew refreshed ground-training proficiency quickly and provided very valuable feedback on sighting positions and improvements to ops products/procedures for upcoming sessions. The crew also noted they found it helpful to douse or dim nearby lighting in the Cupola and Node 3 modules in order to see out the windows without too much internal reflection.

The second session focused on star identification, with each crew member performing a solo 60-minute activity designated $2a$ and $2b$, respectively. Session $2a$ on GMT219 was partially successful

Figure 10. NASA Astronaut Serena Auñón-Chancellor Performing a Sighting Session

in gaining crew proficiency in star identification and sighting with crew member Alex Gerst. The primary science objective of star identification with the new charts was fully accomplished with good crew feedback. The calibration steps were skipped after the camera setup took longer than expected and the measurements began later in the orbit night period. The crew member was able to take 5 sights on 4 star pairs. As a result the secondary science objective for that session (sighting accuracy) was deemed good but indeterminate due to the limited statistical sample. Session $2b$ on GMT220 was successful in gaining crew proficiency in star identification and sighting with crew member Serena Auñón-Chancellor. The primary science objective of star identification with the new charts was fully accomplished with good crew feedback. The instrument calibration was confirmed. The crew member was able to take 7 sights on 3 star pairs with good repeatability. The secondary science objective of evaluating sighting accuracy was achieved with the repeated measurements.

The third session focused on measurement accuracy, with each crew member performing a solo 60-minute activity designated $3a$ and $3b$, respectively. Session $3a$ on GMT227 was conducted with crew member Alex Gerst, and the primary science objective of proficiency and sighting accuracy was fully accomplished. The crew member was able to take 8 sights on 4 star pairs with good repeatability. The average measurement accuracy for the session was 24 arcsec with 16.8 arcsec standard deviation, well within the 60 arcsec expectation. Session $3b$ on GMT232 was successful with crew member Serena Auñón-Chancellor, and again the primary science objective of proficiency and baseline sighting accuracy was fully accomplished. She was able to take multiple star pair readings with good repeatability. The average measurement accuracy was 28 arcsec with 28.4 arcsec standard deviation, also well within the 60 arcsec expectation. These two activities provided confidence the crew was ready to proceed with formal evaluation of sighting positions later that week.

The fourth session focused on sighting position. Session 4 on GMT235 was a single, joint activity conducted by both crew members. The primary science objective of stable sighting position identification and documentation was fully accomplished. The crew members were able to evaluate multiple positions, photograph, and provide feedback on strengths and weaknesses of each. Measurements taken during the orbit night pass were good and consistently within the 60 arcsecond expectation. This activity provided confidence that the crew was ready to proceed with formal evaluation of sighting accuracy in the next session.

The fifth session focused on overall performance, which was executed as two joint activities with one crew member taking sightings and the other documenting results. Session $5a$ on GMT243 was successful with Serena as the operator and Alex photographing the instrument to document the readings. Measurements taken during the orbit night pass showed good repeatability in bias (60 arsec) and a 45 arcsec standard deviation, well within the 60 arcsec expectation for this session. At the end of this session Alex was able to take a sight of the Moon and Mars, which was accurate and good practice for actual lunar distance sights. Session $5b$ on GMT246 was successful, and the primary science objective of formal sighting accuracy evaluation was fully accomplished with the most productive session to date. Alex was the operator, and Serena was able to photograph the instrument to document the readings. Measurements taken during the orbit night pass showed excellent repeatability and accuracy. Measurement bias was 36 arsec with 21 arcsec standard deviation, well within the 60 arcsec expectation for this session.

A bonus sixth session provided the opportunity to take moon limb/diameter measurements. The angular separation between a star/planet and the perpendicular limb of the moon was the primary measurement, historically called the method of lunar distances. For this session, Jupiter was used as the lunar limb target. Session $6a$ on GMT285 was successful, as the primary science objective of sighting using this method was fully accomplished. This session also served to rehearse the technique that would be used for Orion cislunar navigation. Alex was the operator and Serena was able to mark the timetags and photograph the instrument to document the readings. Timetags were more critical for this session as the star-moon geometry changes due to motion of the moon and the observer's spacecraft, unlike star-star pairs. A wristwatch was synchronized prior to the activity and a timetag was noted for each measurement, assumed to be accurate within 2-3 seconds and contributing approximately 5 arsec of additional measurement error. Even with window refraction and timetage errors, measurement bias was 6.9 arsec with 20.2 arcsec standard deviation, well within the 60 arcsec expectation for this session. When the ISS crew rotation did not occur due to the Soyuz abort on October 11, the on-orbit crew schedules had to be understandably re-planned and Session $6b$ was unfortunately canceled.

DATA COLLECTION AND RESULTS

Results were collected via the crew voicing measurements over the communications loop and photographing the sextant drum scale for cross-check on the ground as seen in Figure 11. Based on the 2015 ground test study,[9] the inherent instrument/operator accuracy was expected to have a standard deviation around 20-40 arcsec. With the addition of window refraction and other effects, the expectation for this ISS study was to have measurement standard deviation around 60 arcsec.

It was assumed that window refraction would be a major contributor to the error. The small amount of side error also likely contributed a few arcseconds of error. A classic *Tukey*[10] box-and-whisker plot was constructed using the data from session three and subsequent, the point at which the crew appeared to demonstrate sufficient proficiency with the instrument. Figure 12 shows this result, with 1.5 times the Interquartile Range (IQR) used to identify outliers. In the data for this study, one crew member had two outliers, the other had none. This was actually a useful result, as it showed that outliers were easily identified from standard statistical methods and are likely to be automatically rejected by a navigation filter residual edit check. Both crew members had a noticeable positive bias trend in the measurements, which is consistent with window refraction and side error effects. For convenient use in subsequent covariance analysis, a normal distribution fit with outliers removed was performed as shown in Figure 13. The mean values from these fits for

Figure 11. Sample Photo of Sextant Drum Scale During Sighting Session

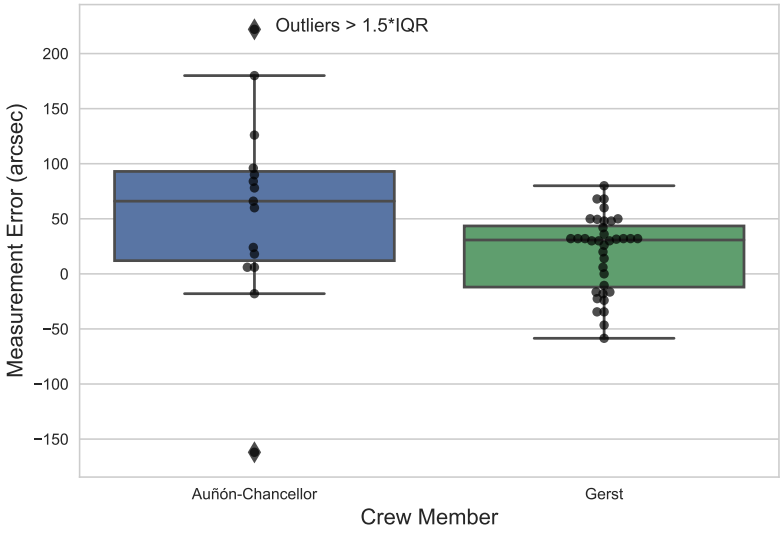

Figure 12. Sighting Statistics Box Plot, 25%-75% Quartile, Outliers>1.5*IQR

the two crew members were 19.4 and 62.8 arcsec, while the standard deviations were 34.2 and 53.2 arcsec. This data supports the original estimates of 60 arcsec standard deviation on the errors. The raw errors by measurement numbers are shown in Figure 14, with outliers identified. Crew member Gerst was able to take several more measurements during session 5 and was the only one with the opportunity to perform session 6, thus more measurements are shown and available for analysis. For Gerst, the repeatability and spread of the measurements did seem to improve with additional sights.

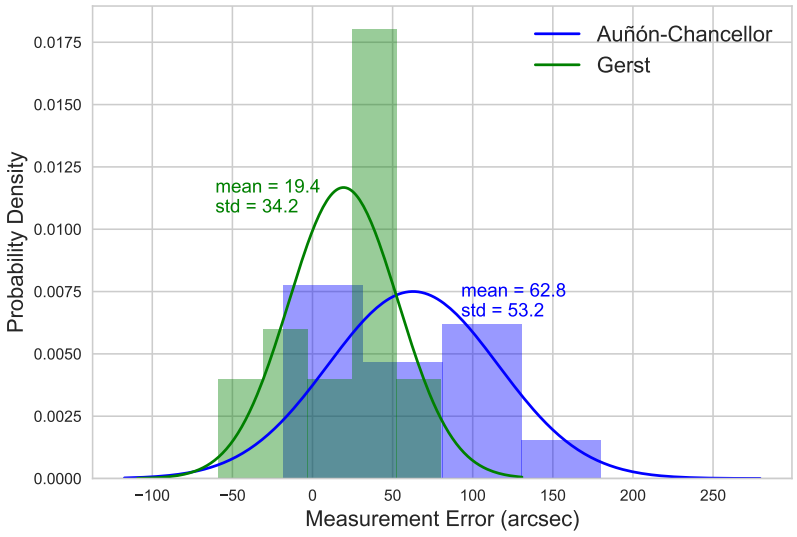

Figure 13. Distribution of Measurement Errors

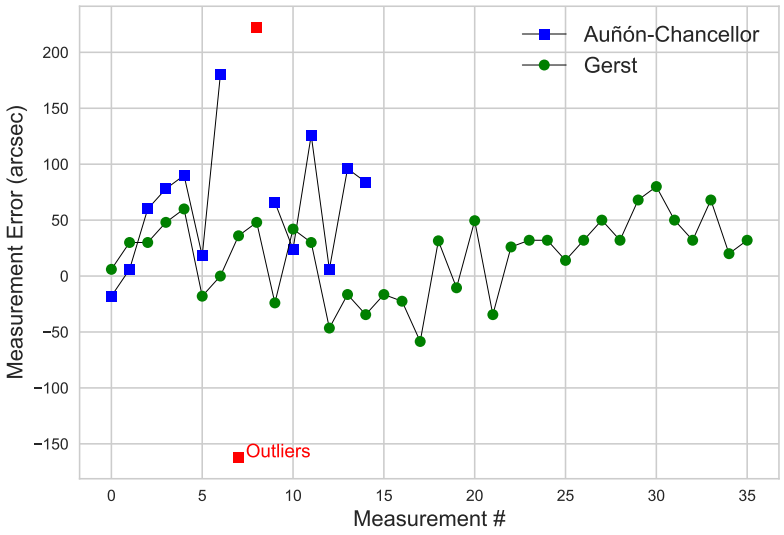

Figure 14. Statistics By Measurement Number

SIMULATION

To further demonstrate the feasibility of sextant measurements for cisulunar navigation, a representative lunar exploration-class trajectory was simulated and a linear covariance (linCov) analysis performed to assess navigation and trajectory dispersion performance. The results demonstrate that navigation solutions would be feasible for performing midcourse corrections to achieve an acceptable entry corridor for emergency crew return. The sextant mathematical measurement model and

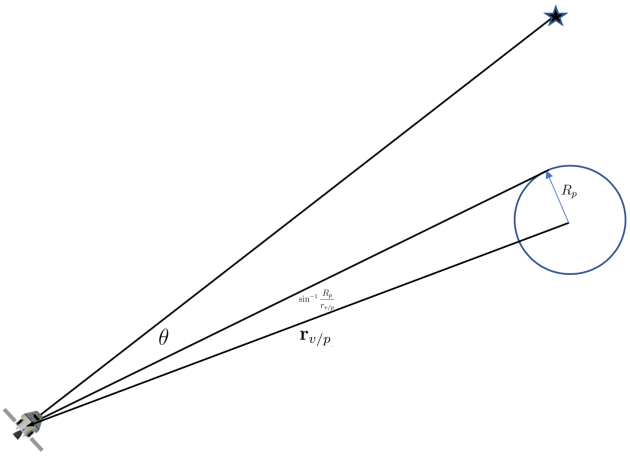

Figure 15. The Sextant Measurement

error modeling is detailed in the following section.

The Sextant Measurement Geometry

The sextant instrument measures the angle between two points. The points could be either two stars or a star and a point on the planetary horizon. Given the unit vector of a star in inertial space, $\mathbf{u}_s$, we take into account stellar aberration which is due to the change of the observer's inertial frame of reference as

$$\mathbf{u}_s^* = \text{Unit}\left(\mathbf{u}_s + \frac{\mathbf{v}_{v/s}}{c}\right) \tag{1}$$

where $\mathbf{v}_{v/s}$ is the inertial velocity of the vehicle with respect to the Sun and c is the speed of light and is related to the so-called *Lorentz transformation.*

For optical navigation in translunar space, the sextant measures the angle between a star and a point on the horizon of the target planet. Given the location of a vehicle with respect to a planet, $\mathbf{r}_{v/p}$ and a point on the horizon, $\mathbf{r}_{h/p} = \mathbf{r}_h$, the unit vector from the vehicle to horizon, $\mathbf{u}_h$ is

$$\mathbf{u}_h = \text{Unit}\left(\mathbf{r}_{h/p} - \mathbf{r}_{v/p}\right) = \frac{\mathbf{r}_{h/p} - \mathbf{r}_{v/p}}{\left|\mathbf{r}_{h/p} - \mathbf{r}_{v/p}\right|} \tag{2}$$

Likewise the correction to the horizon direction due to motion of the observer's frame is

$$\mathbf{u}_h^* = \text{Unit}\left(\mathbf{u}_h + \frac{\mathbf{v}_{v/p}}{c}\right) \tag{3}$$

where here $\mathbf{v}_{v/p}$ is the inertial velocity of the vehicle with respect to the target planet.

With this in hand, the angle between the horizon and the star is found to be

$$\theta = \cos^{-1}(\mathbf{u}_s^* \cdot \mathbf{u}_h^*) \tag{4}$$

This is seen in Figure 15.

The Sextant Measurement Model Errors

The sextant angle measurement is corrupted by various sources of error and these are categorized into three types: instrument error, horizon sighting error, and substellar sighting error. These errors are mathematically modeled in terms of two sources: a zero-mean Gaussian noise sequence (with specified variance) and an Exponentially (time-)Correlated Random Variable (ECRV) (or First-Order Gauss-Markov (FOGM)) processes parameterized by a steady state value and time constant.

The instrument errors are labeled as ν_{sxt} and η_{sxt}; the horizon sighting errors are ν_h and η_h; and the substellar sighting errors are ν_{ss} and η_{ss}. The ECRV errors corresponding to each of these three errors are

$$\dot{\eta}_{sxt}(t) = -\frac{1}{\tau_{sxt}}\eta_{sxt}(t) + w_{sxt}(t), \qquad E(w_{sxt}(t)w_{sxt}(\zeta)) = 2\frac{\sigma^2_{sxt_{ss}}}{\tau_{sxt}}\,\delta(t-\zeta) \tag{5}$$

$$\dot{\eta}_{h}(t) = -\frac{1}{\tau_{h}}\eta_{h}(t) + w_{h}(t), \qquad E(w_{h}(t)w_{h}(\zeta)) = 2\frac{\sigma^2_{h_{ss}}}{\tau_{h}}\,\delta(t-\zeta) \tag{6}$$

$$\dot{\eta}_{ss}(t) = -\frac{1}{\tau_{ss}}\eta_{ss}(t) + w_{ss}(t), \qquad E(w_{ss}(t)w_{ss}(\zeta)) = 2\frac{\sigma^2_{ss_{ss}}}{\tau_{ss}}\,\delta(t-\zeta) \tag{7}$$

where δ is a Dirac delta and $\sigma^2_{(\cdot)_{ss}}$ corresponds to the steady state variance of each of these ECRVs.

For what follows we define the three error sources, instrument, horizon sighting and substellar sighting, as

$$\epsilon_{sxt} \triangleq \nu_{sxt} + \eta_{sxt} \tag{8}$$

$$\epsilon_{h} \triangleq \nu_{h} + \eta_{h} \tag{9}$$

$$\epsilon_{ss} \triangleq \nu_{ss} + \eta_{ss} \tag{10}$$

where the horizon sighting error, ϵ_h, and the substellar sighting error, ϵ_{ss}, are depicted in Figure 16.

We note that in Figure 16 that the errors are small and therefore we use the Law of Cosines to account for all the above errors so that the sextant observation is

$$\begin{aligned}
\mathbf{z}_{sxt} &= \left\{ \left[\theta + \sin^{-1}\frac{R_p}{r_{v/p}}\right]^2 + \left[\sin^{-1}\frac{R_p}{r_{v/p}} + \sin^{-1}\left(\frac{\epsilon_h}{r_{v/p}}\right)\right]^2 \right. \\
&\quad \left. -2\left[\theta + \sin^{-1}\frac{R_p}{r_{v/p}}\right]\left[\sin^{-1}\frac{R_p}{r_{v/p}} + \sin^{-1}\left(\frac{\epsilon_h}{r_{v/p}}\right)\right]\cos(\epsilon_{ss})\right\}^{\frac{1}{2}} + \epsilon_{sxt} \qquad (11) \\
&= \left\{ \left[\theta + \sin^{-1}\frac{R_p}{r_{v/p}}\right]^2 + \left[\sin^{-1}\frac{R_p}{r_{v/p}} + \sin^{-1}\left(\frac{\nu_h+\eta_h}{r_{v/p}}\right)\right]^2 \right. \qquad (12) \\
&\quad \left. -2\left[\theta + \sin^{-1}\frac{R_p}{r_{v/p}}\right]\left[\sin^{-1}\frac{R_p}{r_{v/p}} + \sin^{-1}\left(\frac{\nu_h+\eta_h}{r_{v/p}}\right)\right]\cos(\nu_{ss}+\eta_{ss})\right\}^{\frac{1}{2}} + \nu_{sxt} + \eta_{sxt}
\end{aligned}$$

For what follows we define the state vector $\boldsymbol{\chi}$ as

$$\boldsymbol{\chi} \triangleq \begin{bmatrix} \mathbf{x} \\ \boldsymbol{\eta} \end{bmatrix} \tag{13}$$

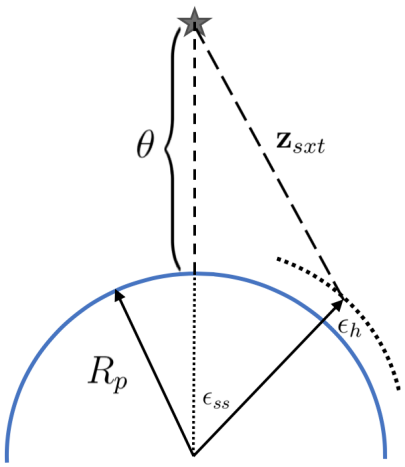

Figure 16. The Sextant Measurement Errors

where $\mathbf{x}$ and $\boldsymbol{\eta}$ are further defined as

$$\mathbf{x} \triangleq \begin{bmatrix} \mathbf{r}_{v/p} \\ \mathbf{v}_{v/p} \\ \boldsymbol{\phi}_B \end{bmatrix} \tag{14}$$

$$\boldsymbol{\eta} \triangleq \begin{bmatrix} \eta_{sxt} \\ \eta_h \\ \eta_{ss} \end{bmatrix} \tag{15}$$

and the noise vector $\boldsymbol{\nu}$ is

$$\boldsymbol{\nu} \triangleq \begin{bmatrix} \nu_{sxt} \\ \nu_h \\ \nu_{ss} \end{bmatrix} \tag{16}$$

The above measurement model is nonlinear and not affine in the measurement errors; therefore the measurement partials are

$$\mathbf{H}_{sxt} = \left.\frac{\partial \mathbf{z}_{sxt}}{\partial \boldsymbol{\chi}}\right|_{\boldsymbol{\chi}=\bar{\boldsymbol{\chi}}} = \begin{bmatrix} \left.\frac{\partial \mathbf{z}_{sxt}}{\partial \mathbf{x}}\right|_{\mathbf{x}=\bar{\mathbf{x}},\boldsymbol{\eta}=\bar{\boldsymbol{\eta}}=\mathbf{0}} & \left.\frac{\partial \mathbf{z}_{sxt}}{\partial \boldsymbol{\eta}}\right|_{\mathbf{x}=\bar{\mathbf{x}},\boldsymbol{\eta}=\bar{\boldsymbol{\eta}}=\mathbf{0}} \end{bmatrix} \tag{17}$$

$$\tag{18}$$

and the measurement noise mapping matrix, $\mathbf{L}_{sxt}$, is

$$\mathbf{L}_{sxt} = \left.\frac{\partial \mathbf{z}_{sxt}}{\partial \boldsymbol{\nu}}\right|_{\boldsymbol{\nu}=\bar{\boldsymbol{\nu}}=\mathbf{0}} \tag{19}$$

so that the measurement noise used in the filter is

$$\mathbf{R}_{sxt} = \mathbf{L}_{sxt} E\left(\boldsymbol{\nu}\boldsymbol{\nu}^T\right) \mathbf{L}_{sxt}^T \tag{20}$$

Simulation Results

For this sample lunar flyby mission simulation, the simulated passes were 12 minutes long with measurements taken twice per minute. The passes were twice per day and before each of 4 outbound and 3 inbound midcourse correction maneuvers. The errors were

$$\epsilon_{sxt} = 60 \text{ arcsec}, 1\sigma \quad (21)$$

$$\epsilon_{h} = 10 \text{ arcsec}, 1\sigma \quad (22)$$

$$\epsilon_{ss} = 10 \text{ arcsec}, 1\sigma \quad (23)$$

where the instrument/operator errors, ϵ_{sxt}, came from this ISS experiment and the horizon sighting error, ϵ_h, and substellar sighting error, ϵ_{ss}, are depicted in Figure 16. For conservatism the sextant measurements are simulated for the entire mission without any external updates, although for emergency use the navigation state would likely be better conditioned by previous ground-based radiometric updates before using the sextant. The simulation is run all the way to entry interface, and the resulting dispersions in the trajectory are evaluated against acceptable entry conditions. These results are shown as a series of plots in Figure 17. The contingency corridor requirements at entry

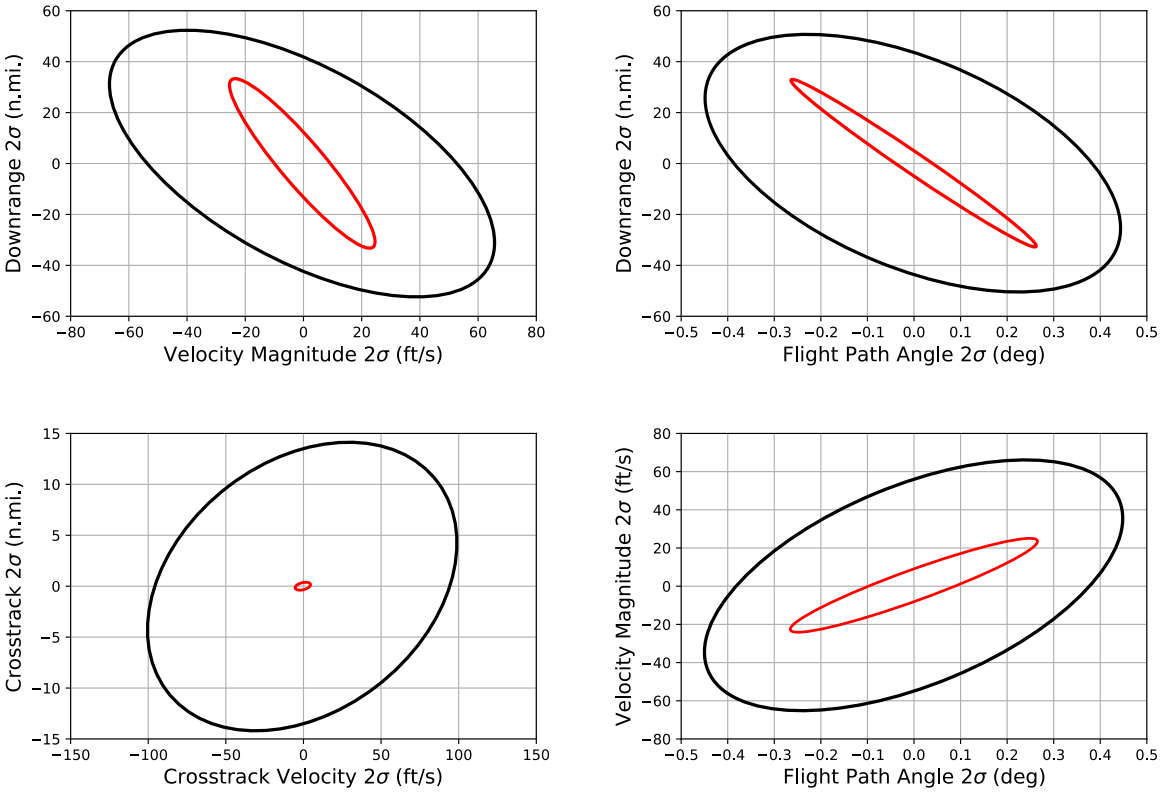

Figure 17. Lincov Entry Interface Dispersions

interface are shown in black, and the simulated spacecraft dispersions are shown in red. These plots show adequate 2σ margin against all parameters and confirm the feasibility of this approach.

CONCLUSION AND FUTURE WORK

Two crew members with different skills, background, and ability were able to produce quality sights on-orbit through a spacecraft window with minimal training and practice. This supports the feasibility of a sextant for emergency cislunar navigation from the perspective of measurement accuracy. No extraordinary provision was made to minimize window refraction effects other than generally preferring sights near the center rather than edges of a window.

Future work in this area could certainly include data from additional crew members. As of the writing of this paper, the sextant is still onboard ISS and could be utilized again. A key improvement in the sighting performance seemed to be gained when the scope was refocused between sights, especially out different windows, and this will be added to the standard procedure for sighting. The two adjustment tools need to be attached to the sextant with a lanyard or similar to make them easier to manipulate and prevent loss. The crew also needs to practice making mirror adjustments on the ground with these tools. A small red LED light for reading measurements would be beneficial. As noted before, the crew needs sighting products with the moon or Earth as a reference for finding nearby stars. Additionally, trying to adjust the sight to be in the center of the window or applying a compensation for edge of window refraction could provide small improvements.

ACKNOWLEDGMENTS

The authors wish to acknowledge and thank ESA astronaut Alexander Gerst and NASA astronaut Serena Auñón-Chancellor for their enthusiastic support and participation in this study. Additionally, thanks are due to payload support team members Brandon Williams, Kristen Fortson, Burgess Howell, Robert Waymire, Sadie Holbert, and Heather Love. Training assistance Amy Efting and Jonathan Zahn. Lincov assistance Chris D'Souza.

REFERENCES

[1] K. Nordtvedt, "A Theory of Manual Space Navigation," NASA CR-841, Montana State University, March 1967.

[2] C. Havill, "An Emergency Midcourse Navigation Procedure for a Space Vehicle Returning From the Moon," NASA TN-D-1765, NASA Ames Research Center, March 1963.

[3] R. Zanetti, "Autonomous Midcourse Navigation for Lunar Return," *Journal of Spacecraft and Rockets*, Vol. 44, July-August 2009, pp. 865–873.

[4] B. A. Lampkin and R. J. Randle, "Investigation of a Manual Sextant-Sighting Task in the Ames Midcourse Navigation and Guidance Simulator," Tech. Rep. NASA TN D-2844, NASA Ames Research Center, May 1965.

[5] D. W. Smith, "Hand-Held Sextant: Results from Gemini XII and Flight Simulator Experiments," *J. Spacecraft*, Vol. 5, June 1968, pp. 655–662.

[6] R. H. Battin, *Astronautical Guidance*. McGraw-Hill, Inc., 1964.

[7] P. J. Brennan and I. S. Johnson, "Manually-Aided On-Board Apollo Cislunar Navigation," *Proceedings of the Twenty-Fight Anniversary Year Meeting*, Colorado Springs, CO, Institute of Navigation, July 1970.

[8] T. M. Eneev, V. V. Ivashkina, V. A. Sharov, and J. V. Bagdasarya, "Space autonomous navigation system of Soviet project for manned fly by Moon," *Astra Astronautica*, Vol. 66, 2009, pp. 341–347.

[9] B. Wood and G. Holt, "Orion Sextant Performance Testing and Analysis," FltDyn-CEV-15-42, NASA Johnson Space Center, September 2015.

[10] J. Tukey, *Exploratory Data Analysis*. Addison-Wesley, 1977.